IEEE Access
Multidisciplinary | Rapid Review | Open Access Journal

Received March 5, 2020, accepted March 19, 2020, date of publication March 30, 2020, date of current version April 29, 2020.

Digital Object Identifier 10.1109/ACCESS.2020.2983998

A Takagi-Sugeno Fuzzy Model-Based Control Strategy for Variable Stiffness and Variable Damping Suspension

XIN TANG[1], (Member, IEEE), DONGHONG NING[2], (Member, IEEE), HAIPING DU[2], (Senior Member, IEEE), WEIHUA LI[3], (Member, IEEE), YIBO GAO[4], AND WEIJIA WEN[1,4]

[1]Guangzhou HKUST Fok Ying Tung Research Institute, Guangzhou 511458, China
[2]School of Electrical, Computer and Telecommunications Engineering, University of Wollongong, Wollongong, NSW 2522, Australia
[3]School of Mechanical, Materials, Mechatronic and Biomedical Engineering, University of Wollongong, Wollongong, NSW 2522, Australia
[4]Department of Physics, Hong Kong University of Science and Technology, Hong Kong

Corresponding author: Xin Tang (xintang@ust.hk)

This work was supported in part by the China Postdoctoral Science Foundation under Grant 2019M662847 and in part by the Guangzhou Postdoctoral International Training Program.

ABSTRACT As the concept of variable stiffness and variable damping (VSVD) has increasingly drawn attention, suspensions applied with magnetorheological (MR) dampers to achieve varying stiffness and damping have been an attractive method to improve vehicle performance and driver comfort further. As highly nonlinearity of MR damper dynamics and coupled interconnections in the case of multi-output control, to build a direct control system for VSVD suspension based on multiple MR dampers is difficult. Applying Takagi-Sugeno (T-S) fuzzy model on the VSVD system enables the linear control theory to be directly utilized to build the multi-output controller for multi-MR dampers. In this paper, a T-S fuzzy model is established to describe an MR VSVD suspension model, and then an H∞ controller that considers the multi-input/multi-output (MIMO) coupled interconnections characteristic and multi-object optimization is designed. To estimate state information for the T-S fuzzy model in real-time, a state observer is designed and integrated in the controller. Then, the performance of the VSVD control algorithm was evaluated by numerical simulation. The results demonstrate that the T-S fuzzy model-based H∞ controller outperforms the independent control method for a VSVD suspension system with multi-MR dampers.

INDEX TERMS MIMO, robust control, Takagi-Sugeno fuzzy model, variable stiffness and variable damping.

I. INTRODUCTION

Vehicle suspension is used to provide ride comfort, road holding, and other dynamic functions such as supporting the vehicle weight and maintain vehicle height. To date, active and semi-active instruments are two typical methods used to improve vehicle suspension performance [1]. Despite that active control performs better at reducing vibrations, the disadvantages of potential instability and large power consumption limit its common use. On the contrary, semi-active suspensions offer a desirable performance enhanced by active suspensions without requiring high power consumption and expensive hardware [2]. Magnetorheological (MR) dampers are semi-active devices that use MR fluids to provide controllable damping forces while requiring only battery power. An MR damper is used most widely in vehicle suspension [3] as a nonlinear component and its corresponding control strategies has been studied by many researchers in recent years. A variety of control algorithms, such as clipped optimal control, skyhook control, sliding mode control, neural network control, fuzzy logic control, gain-scheduled control and $H\infty$ control, have been proposed for MR damper to conduct vehicle suspension's damping adjustment [4], [5].

Apart from suspension damping, stiffness is another important component that affects the performance of a suspension. To date, passive spring has been widely used in vehicle suspension. However, it cannot satisfy the conflicting requirement of improved both ride comfort and driving stability.

The associate editor coordinating the review of this manuscript and approving it for publication was Ning Sun.

An idealized suspension spring is supposed to be controllable so as to provide different stiffness values depending on the specific driving and road conditions. For this requirement, the concept of variable stiffness has been integrated into damping variable suspension system to form a variable stiffness and variable damping (VSVD) suspension system. Based on this motivation, our group developed a full-scaled MR suspension system with tunable stiffness and damping characteristics and the dynamic effectiveness has been proved. Furthermore, a simple but proper on-off control algorithm for the advanced suspension system has been developed in [6]. Till now, the research area of the VSVD control is still largely unexplored; most of them still are focusing on VSVD control mechanism [7], [8], just a few works propose the specific feasible controller on this topic. In [9], [10], Xu *et al.* proposed a hybrid control strategy for a VSVD suspension to improve vehicle lateral stability. The control strategy composed of a fuzzy controller that the output is wheel slip ratio and an on-off controller to improve normal force at the tyre. The simulation result verifies their usefulness in enhancing vehicle stability by replacing a passive front suspension system with a hybrid control-based variable stiffness and damping structure. In an active VSVD system, a control algorithm [11] proposed by Anubi *et al.* applies the concept of nonlinear energy sink to effectively transfer the vibrational energy in the sprung mass to a control mass. This skyhook-based concept can reduce the vibration from road disturbance to the car body at a relatively lower cost than a traditional variable damping active suspension. In addition, Aunbi *et al.* further reported a corresponding semi-active structure for suspension system in [12]. The performance of the controller based on the nonlinear energy sink concept has been verified by simulation work. In this case, the control algorithm is applied to a horizontal MR damper in a McPherson suspension structure to adjust the corresponding stiffness value. Furthermore, Spelta *et al.* developed a VSVD controller considering the critical trade-off between the choice of the stiffness coefficient and the end-stop hitting to improve the riding comfort of vehicles further [13]. The simulation result demonstrates that the variable stiffness and damping suspension controlled by their control algorithm improves vibration isolation better than suspensions with only variable damping.

It is noticed from all the past and present studies that different control algorithms have different advantages with respect to different aspects of performance, and the performance of the controlled device is highly dependent on the choice of the control algorithm and the nonlinear complexity of the dynamic model. To solve the nonlinear issue in modeling, Yang *et al.* presented a neural network-based adaptive control method [14] that can provide effective control based on the original nonlinear dynamics without any linearizing operations. Furthermore, by adding some designed nonlinear terms and introducing the concept of lumped mass method and virtual spring in the dynamic model, the controllers in [15], [16] can also provide the closed-loop asymptotic stability without any linearization for the original model.

Till now, researchers have found that the good vibration reduction effectiveness is often controlled by the system using variable stiffness to reduce the low frequency responses of sprung mass accelerations and using variable damping to reduce the high frequency responses of wheel load fluctuations, respectively [17]. In the real-time VSVD control, however, the damping value and stiffness value in suspension system are complementary and coupled to each other. It is caused by the coupled interconnections between the time varying damping and the time varying stiffness, which have led to the fluctuation of the value of solution [18]. It is also noted that the above articles that most of the control methods just using two independent controllers based on the single on-off control method to deal with the structure's variable stiffness and variable damping work. There are two problems to attenuate the effect of shock absorption in these control strategies. First, the simple on-off control method does not adequately consider the nonlinear characteristics of MR damper; second, the independent control method for stiffness module and damping module cannot effectively overcome the coupled interconnections characteristic of multiple outputs of the system. Indeed, as high nonlinearity of MR damper dynamics and coupled interconnections characteristic in multi-input-multi-output (MIMO) control system, to build a direct control system for a VSVD suspension with multiple MR dampers is difficult.

At present, although direct robust control has been widely used in vibration semi-active control, most of them are designed for single-input and single-output control system and bare researches are applied to MIMO control system [19]. In fact, $H\infty$ theory regarding as a robust control algorithm is highly suitable to deal with MIMO system [20], [21]. The goal of single output system control is to design a closed-loop controller to realize the shaping of frequency response function; however, applying the similar mothed that to shape every frequency response function to multi-input and the multi-output system is difficult and unfeasible. By defining $H\infty$ norm of transfer function matrix and then shaping $H\infty$ norm in the frequency domain, $H\infty$ theory can be applied to deal with the control problem in MIMO system well. Currently, a robust mixed-sensitivity $H\infty$ output feedback controller by using loop shaping with regional pole placement for MIMO nonlinear system was studied in [22]. More recently, an $H\infty$ output feedback controller for a class of time-delayed MIMO nonlinear systems was presented in [23]. However, the above control methods, no matter whether they were proposed for vehicle suspensions or structural vibration control, normally compute/design the desired damping force without considering the device's highly nonlinear dynamics. As a matter of fact, it is very important to be considered to deal with high nonlinearity of dynamic model in a MIMO system with multiple MR dampers. The algorithm which is capable of solving the coupling effect and high nonlinearity of a multi-MR damper control system has rarely been developed, although papers have verified the superiority of controllers' performance for a single MR damper system.

Based on this motivation, this paper will propose a Takagi-Sugeno fuzzy model-based $H\infty$ (TSFH) VSVD control strategy so that the nonlinear dynamic characteristics of the VSVD suspension's two MR dampers can be both considered in the controller design and the desired control performance can be realized for a practical system. Different from the existing control strategies, the proposed algorithm can effectively solve the joint control issue of a multi-MR nonlinear system by integrating a double Bouc-Wen T-S fuzzy model and a multi-object-optimized $H\infty$ controller. Furthermore, different from the study of [24], where the fuzzy model of a VSVD suspension was identified by training the input-output data sets and the accuracy was fully dependent on expert experience in selecting appropriate fuzzy sets and fuzzy rules, the T-S fuzzy model of a VSVD suspension will be obtained in this paper by considering a proposed suspension's double Bouc-Wen MR damper model and using the approach of 'sector nonlinearity' [25]. Further discussion on robust multi-objective controller design, taking into consideration the coupled interconnections of multi-output [26], the hysteresis of multi-MR dampers, and the vehicle suspension performance requirements on ride comfort, road holding, and suspension deflection [27], is also provided. Based on the $H\infty$ controller integrating multi-objective optimization, both the closed-loop system stability and the closed-loop performance can be theoretically guaranteed. Further considering the case that not all the state variables, in particular, the evolutionary variable used to describe the MR damper dynamics by the Bouc-Wen model, are available by measurement in practice, a state observer is designed and integrated into the controller to obtain the estimated premise and state variables. Then, based on the MR VSVD suspension's dynamic characterization in [28], numerical simulations are used to validate the effectiveness of the proposed approach.

The rest of this paper is organized as follows. Section II presents the VSVD suspension's working principle and its dynamic model. The T-S fuzzy modeling process of the VSVD suspension and the design of the observer and controller are described in section III. Section IV presents the numerical simulation and the results are discussed in time and frequency domains. Finally, our findings are concluded in section V.

II. PRELIMINARIES

The proposed controller will be designed based on a quarter-car model with the MR VSVD suspension. The working principle of the applied VSVD suspension is introduced in section II-A. Then, to develop a real-time controller, section II-B gives the phenomenological model of the MR VSVD suspension, and integrates it into the quarter-car model. In section II-C, the integrated quarter-car model is described by state-space equations to conduct the preliminary of control design.

A. THE WORKING PRINCIPLE OF THE VSVD SUSPENSION

The working principle of the variable stiffness and damping suspension can be demonstrated by Fig. 1(a), where three

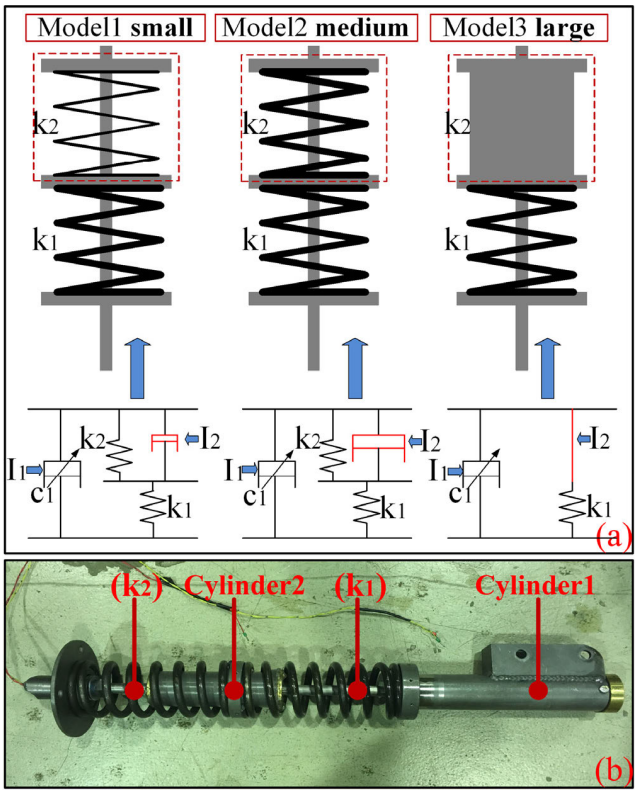

FIGURE 1. (a) The MR VSVD suspension working principle and (b) structure configuration.

different connection modes of this device are illustrated, and Fig. 1(b) shows the structure of the system. When the current I_2 applied to the upper stiffness cylinder 2 is small enough, the cylinder's damping force will allow the relative motion between the shaft and cylinder 2. In this case, the VSVD suspension is working in connection mode 1 where the spring k_1 and the spring k_2 work in series because both springs deform when the cylinder 2 slides along the shaft. When the current I_2 becomes bigger, the device will work in connection mode 2. In this working mode, the larger damping force makes the sliding motion between the cylinder 2 and shaft harder and slower. It is equivalent to the growth of the stiffness value of the spring k_2.

Furthermore, when the upper cylinder's damping force is large enough to prevent the relative motion between the cylinder and the centre shaft, the VSVD suspension is working in connection mode 3, because only spring k_1 will have a deformation in response to the external force. The determination of connection mode is controlled by the magnitude of the upper damping force, which is determined by the amount of the input current I_2. The stiffness variability, therefore, is realised by the switch between the connection modes. The damping variability is realized by adjusting the current I_1 applied to the lower damping cylinder 1. As shown in Fig. 1(a), no matter which connection mode the VSVD suspension is, the overall equivalent damping is represented by the damping c_1. c_1 increases as the current I_1 applied to the cylinder 1 increases.

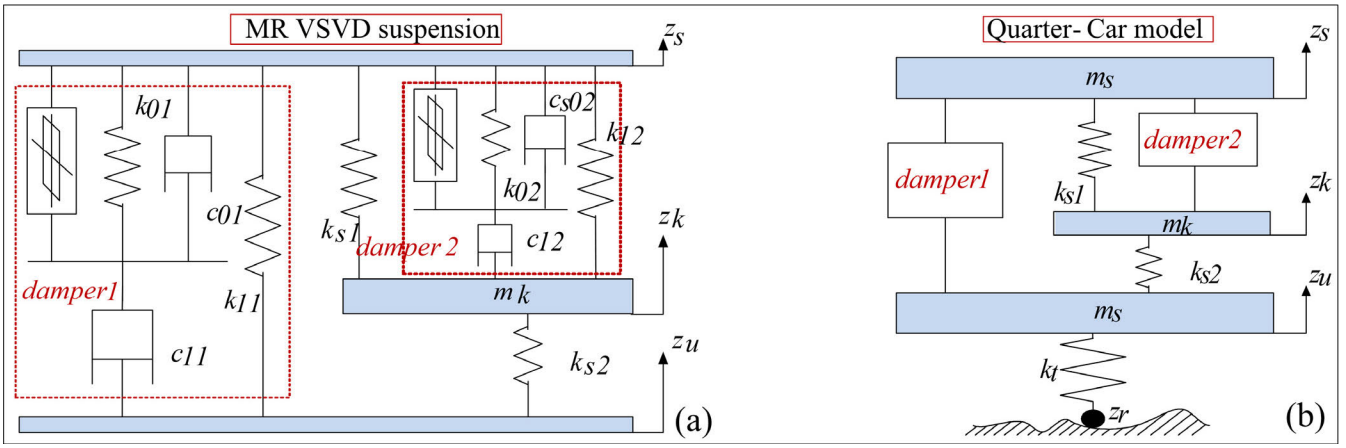

FIGURE 2. Schematic diagram of (a) the proposed MR VSVD suspension model and (b) the quarter-car model with the MR VSVD suspension.

In summary, the effective stiffness of the proposed VSVD suspension is controlled by current I_2 and the equivalent damping is controlled independently by current I_1.

B. THE QUARTER-CAR MODEL WITH THE MR VSVD SUSPENSION

The Bouc-Wen model has been widely accepted in describing MR behavior for its mathematical simplicity and accuracy but with unmeasurable state variables [29]. In real-time control, a simplified Bouc-Wen model is suggested to be applied, which has less and measurable state variables (the unmeasurable state variable y in Bouc-Wen model is replaced), but also the accuracy to describe the hysteretic behavior of an MR structure.

To implement the real-time controller design, the proposed MR VSVD suspension phenomenological model in this section is integrated with two simplified Bouc-Wen models, and Fig. 2(a) shows the schematic diagram of the proposed model. The mathematical description for this model is as follows:

$$\begin{aligned} F &= F_d + k_{s1}(z - z_k) + F_s, \\ F_d &= \alpha_1 z_{d1} + k_{01} \cdot z + C_{01} \cdot \dot{z}, \\ F_s &= \alpha_2 z_{d2} + k_{02}(z - z_k) + C_{02}(\dot{z} - \dot{z}_k), \\ m_k \ddot{z}_k &= F_s + k_{s1}(z_k - z) - k_{s2} \cdot z_k, \end{aligned} \tag{1}$$

where

$$\begin{aligned} \dot{z}_{d1} &= -\gamma_1 |\dot{z}| \cdot z_{d1} |z_{d1}| - \beta_1 \cdot \dot{z} \cdot \dot{z}_{d1}^2 + A_{d1}(\dot{z}), \\ \dot{z}_{d2} &= -\gamma_2 |\dot{z} - \dot{z}_k| \cdot z_{d2} \cdot |z_{d2}| - \beta_2 (\dot{z} - \dot{z}_k) z_{d2}^2 \\ &\quad + A_{d2}(\dot{z} - \dot{z}_k), \\ \alpha_1 &= \alpha_{1a} + \alpha_{1b} \cdot I_1, \\ C_{01} &= C_{01a} + C_{01b} \cdot I_1, \\ \alpha_2 &= \alpha_{2a} + \alpha_{2b} \cdot I_2, \\ C_{02} &= C_{02a} + C_{02b} \cdot I_2, \end{aligned}$$

and F is the total force generated by the VSVD suspension; F_d and F_s are the force generated by the damper 1 and the damper 2, respectively; $A_{d1}, A_{d2}, \beta_1, \beta_2, \gamma_1$ and γ_2 are used to describe the hysteresis behavior; α_1 and α_2 are the evolutionary coefficient; C_{01} and C_{01} are the viscous damping; k_{s1} and k_{s2} are the spring stiffness; k_{01} and k_{02} are the accumulator stiffness; z and z_k are the displacements of the suspension and the top damper cylinder, respectively; m_k is the mass of the damper 2; I_1 and I_2 are the command currents sent to the MR damper 1 and MR damper 2, respectively.

The linear dynamic model of a quarter-car can be described by the following equations [27]:

$$\begin{aligned} m_s \ddot{z}_s + c_s(\dot{z}_s - \dot{z}_u) + (z_s - x_u) &= 0, \\ m_u \ddot{z}_u + k_t(z_u - z_r) + c_s(\dot{z}_s - \dot{z}_u) - k_s(z_s - x_u) &= 0, \end{aligned} \tag{2}$$

where m_s is the sprung mass; m_u is the un-sprung mass; z_s is the displacement of the sprung mass; z_u is the displacement of the un-sprung mass; z_r represents the road profile; k_t is the tire stiffness, whereas k_s is the stiffness of the spring between the tire and the chassis; c_s is the damping of a passive damper that provides a damping force proportional to the velocity $(\dot{z}_s - \dot{z}_u)$.

The idea is to substitute the linear passive damper with the MR damper to provide variable damping, and to change the linear passive spring to MR spring module to provide variable stiffness. Therefore, the linear quarter-car model is replaced by the one with the MR VSVD suspension model mentioned previously. The applied quarter-car model with the damper and spring replacement is shown in Fig. 2(b).

Substituting (1) into (2) gives the dynamic description of the quarter-car with the MR VSVD suspension as follows:

$$\begin{aligned} m_s \ddot{z}_s &= -[(\alpha_{1a} + \alpha_{1b} I_1) z_{d1} + k_{01}(z_s - z_u) \\ &\quad + (c_{01a} + c_{01b} I_1)(\dot{z}_s - \dot{z}_u) + k_{s1}(z_s - z_k) \\ &\quad + (\alpha_{2a} + \alpha_{2b} I_2) z_{d2} + k_{02}(z_s - z_k) \\ &\quad + (c_{02a} + c_{02b} I_2)(\dot{z}_s - \dot{z}_u)], \\ m_u \ddot{z}_u &= (\alpha_{1a} + \alpha_{1b} I_1) z_{d1} + k_{01}(z_s - z_u) \\ &\quad + (c_{01a} + c_{01b} I_1)(\dot{z}_s - \dot{z}_u) + k_{s1}(z_s - z_k) \\ &\quad - k_t(z_u - z_r), \end{aligned}$$

$$m_k\ddot{k}_u = k_{s1}(z_s - z_k) + (\alpha_{2a} + \alpha_{2b}I_2)z_{d2} - k_{s2}(z_k - z_u) + k_{02}(z_s - z_k) + (c_{02a} + c_{02b}I_1)(\dot{z}_s - \dot{z}_u). \quad (3)$$

Note that the parameter F in (1) is equivalent to $c_s(\dot{z}_s - \dot{z}_u) + k_s(z_s - z_u)$ in (2). It is also noted that the phenomenological model of the VSVD suspension is established based on two Bouc-Wen models, which are numerically tractable. The model's parameters are determined by the experimental data with an appropriate numerical fitting method [28], which are shown in Table 1.

TABLE 1. Parameter Values of the MR VSVD Suspension.

Symbol	Value	Unit	Symbol	Value	Unit
A_{d1}	120	/	A_{d2}	89	/
β_1	237602	m^{-2}	β_2	266259	m^{-2}
γ_1	219872	m^{-2}	γ_2	1277656	m^{-2}
α_{1a}	7211	N / m	α_{1b}	23415	N/m·V
α_{2a}	18654	N / m	α_{2b}	43876	N/m·V
C_{01a}	15036	N·s/m	C_{01b}	11221	N·s/m
C_{02a}	20657	N·s/m	C_{02b}	1876	N·s/m
k_{01}	347	N / m	k_{02}	29032	N / m
k_{s1}	29976	N / m	k_{s2}	38500	N / m
m_k	4.8	kg			

C. STATE-SPACE MODEL FOR REAL-TIME CONTROL

For the process of T-S Fuzzy modeling, the state variables of the quarter-car model are defined as follows:

$$x_1 = \dot{z}_s, \quad x_2 = \dot{z}_u, x_3 = \dot{z}_k, x_4 = z_s - z_u, \quad x_5 = z_k - z_u, \quad x_6 = z_u - z_r, x_7 = z_{d1}, x_8 = z_{d2}, \quad (4)$$

and the state vector as:

$$x = \begin{bmatrix} x_1 & x_2 & x_3 & x_4 & x_5 & x_6 & x_7 & x_8 \end{bmatrix}^T, \quad (5)$$

In order to simplify the highly nonlinearity of the proposed model, define $\widetilde{f_1}, \widetilde{f_2}$ as:

$$\widetilde{f_1} = -\gamma_1 |\dot{z}_s - \dot{z}_u| \cdot z_{d1} \cdot |z_{d1}| - \beta_1 (\dot{z}_s - \dot{z}_u) |z_{d1}|^2,$$
$$\widetilde{f_2} = -\gamma_2 |\dot{z}_s - \dot{z}_u| \cdot z_{d2} \cdot |z_{d2}| - \beta_2 (\dot{z}_s - \dot{z}_u) |z_{d2}|^2. \quad (6)$$

Then define:

$$f_1 = \frac{\widetilde{f_1}}{x_7},$$
$$f_2 = \frac{\widetilde{f_2}}{x_8},$$
$$f_3 = \alpha_{1b} \cdot x_7 + c_{01b}(x_1 - x_2),$$
$$f_4 = \alpha_{2b} \cdot x_8 + c_{02b}(x_1 - x_3). \quad (7)$$

Then, equation (3) can be written as:

$$m_s\dot{x}_1 = -[\alpha_{1a}x_7 + k_{01}x_4 + c_{01a}x_1 - c_{01a}x_2 + f_3I_1 + k_{s1}x_4 - k_{s1}x_5 + \alpha_{2a}x_8 + k_{02}x_4 - k_{02}x_5 + c_{02a}x_1 - c_{02a}x_3 + f_4I_2],$$
$$m_u\dot{x}_2 = \alpha_{1a}x_7 + k_{01}x_4 + c_{01a}x_1 - c_{01a}x_2 + k_{s2}x_5 - k_tx_6 + f_3I_1,$$
$$m_k\dot{x}_3 = k_{s1}x_4 - k_{s1}x_5 + \alpha_{2a}x_8 + k_{02}x_4 - k_{02}x_5 + c_{02a}x_1 - c_{02a}x_3 - k_{s2}x_5 + f_4I_2,$$
$$\dot{x}_4 = x_1 - x_2,$$
$$\dot{x}_5 = x_3 - x_2,$$
$$\dot{x}_6 = x_2 - \dot{z}_r,$$
$$\dot{x}_7 = f_1x_7 + Ad_1(x_1 - x_2),$$
$$\dot{x}_8 = f_2x_8 + Ad_1(x_1 - x_3). \quad (8)$$

We can write a state-space for system (5) as:

$$\dot{x}(t) = Ax + B_1w + B_2u, \quad (9)$$

where the output vector as $u = \begin{bmatrix} I_1 & I_2 \end{bmatrix}^T$, the disturbance vector as $w = z_r$, and the large matrices, A, B_1, and B_2 are listed in appendix for better readability.

In addition, the input currents sent to the MR dampers is practically limited, and therefore the asymmetry saturation of the control signals should be considered. In general, a control input with saturation limitation is defined as $\overline{u} = sat(u)$, where $sat(u)$ is a asymmetry saturation function defined as

$$sat(u) = \begin{cases} u_{\min}, & u < u_{\min}, \\ u, & u_{\min} \le u \le u_{\max}, \\ u_{\max}, & u \ge u_{\max}, \end{cases} \quad (10)$$

where $u_{\min}$ and $u_{\max}$ are the control input limits, and $u_{\min} < u_{\max}$. In particular, the $\overline{u}$ can be described as $\overline{u} = \begin{bmatrix} \overline{I}_1 & \overline{I}_2 \end{bmatrix}^T = \begin{bmatrix} sat(I_1) & sat(I_2) \end{bmatrix}^T$, where

$$sat(I_1) = \begin{cases} I_{1\min}, & I_1 < I_{1\min}, \\ I_1, & I_{1\min} \le I_1 \le I_{1\max}, \\ I_{1\max}, & I_1 \ge I_{1\max}, \end{cases}$$
$$sat(I_2) = \begin{cases} I_{2\min}, & I_2 < I_{2\min}, \\ I_2, & I_{2\min} \le I_2 \le I_{2\max}, \\ I_{2\max}, & I_2 \ge I_{2\max}, \end{cases} \quad (11)$$

and $I_{1\min} < I_{1\max}$ and $I_{2\min} < I_{2\max}$ are the control limits of signals I_1 and I_2, respectively. Therefore, the system (9) can be written as

$$\dot{x}(t) = Ax + B_1w + B_2\overline{u}. \quad (12)$$

III. T-S FUZZY MODEL-BASED H∞ CONTROLLER DESIGN

This section investigates the design of the T-S fuzzy model-based $H\infty$ controller for the quarter-car with MR VSVD suspension. In section III-A, a T-S fuzzy model will be established to describe the integrated quarter-car model. To estimate state information for the T-S fuzzy model in real-time, in section III-B, a state observer will be designed and integrated in the controller. Finally, an $H\infty$ controller for the MIMO system that considers the coupled interconnections characteristic and multi-object optimization process will be designed in section III-C.

A. T-S FUZZY MODELING OF QUARTER-CAR WITH VSVD SUSPENSION

T-S Fuzzy modeling method is applied here to do linear approximation considering the high nonlinearity of the system (8). It is noted that the state variables x_1, x_2, x_3, x_7, and x_8 are actually limited in practice for a stable system, the nonlinear f_1, f_2, f_3, and f_4 should also be bounded in operation. We represent f_1, f_2, f_3, and f_4 using their minimum values and maximum values by following "sector nonlinearity" approach [25]:

$$\begin{aligned} f_1 &= M_1 \cdot f_{1max} + M_2 \cdot f_{1min}, \\ f_2 &= N_1 \cdot f_{2max} + N_2 \cdot f_{2min}, \\ f_3 &= T_1 \cdot f_{3max} + T_2 \cdot f_{3min}, \\ f_4 &= H_1 \cdot f_{4max} + H_2 \cdot f_{4min}, \end{aligned} \tag{13}$$

where $f_{(i)max}$ $(i = 1, 2, 3, 4)$ represents the maximum values and $f_{(i)min}$ $(i = 1, 2, 3, 4)$ is the minimum values of the nonlinear $f_{(i)}$ $(i = 1, 2, 3, 4)$. $M_{(i)}$, $N_{(i)}$, $T_{(i)}$, and $H_{(i)}$ $(i = 1, 2)$ are fuzzy membership functions and satisfy:

$$\begin{aligned} M_1 + M_2 &= 1, \\ N_1 + N_2 &= 1, \\ T_1 + T_2 &= 1, \\ H_1 + H_2 &= 1, \end{aligned} \tag{14}$$

and the member functions are defined as:

$$\begin{aligned} M_1 &= \frac{f_1 - f_{1\min}}{f_{1\max} - f_{1\min}}, \quad M_2 = \frac{f_{1\max} - f_1}{f_{1\max} - f_{1\min}}, \\ N_1 &= \frac{f_2 - f_{2\min}}{f_{2\max} - f_{2\min}}, \quad N_2 = \frac{f_{2\max} - f_2}{f_{2\max} - f_{2\min}}, \\ T_1 &= \frac{f_3 - f_{3\min}}{f_{3\max} - f_{3\min}}, \quad T_2 = \frac{f_{3\max} - f_3}{f_{3\max} - f_{3\min}}, \\ H_1 &= \frac{f_4 - f_{4\min}}{f_{4\max} - f_{4\min}}, \quad H_2 = \frac{f_{4\max} - f_4}{f_{4\max} - f_{4\min}}. \end{aligned} \tag{15}$$

Then the nonlinear quarter-car system can be described by the above linear subsystems. For each possibility, there is a corresponding state-space equation:

$$\begin{aligned} &\text{If } f_1 = M_2, f_2 = N_1, f_3 = T_1, f_4 = H_1, \\ &\qquad \text{then } \dot{x} = A_{(8)}\mathrm{x} + B_1 w + B_{2(8)}\bar{u}. \\ &\text{If } f_1 = M_2, f_2 = N_2, f_3 = T_1, f_4 = H_1, \\ &\qquad \text{then } \dot{x} = A_{(9)}\mathrm{x} + B_1 w + B_{2(9)}\bar{u}. \\ &\text{If } f_1 = M_2, f_2 = N_2, f_3 = T_2, f_4 = H_1, \\ &\qquad \text{then } \dot{x} = A_{(10)}\mathrm{x} + B_1 w + B_{2(10)}\bar{u}. \\ &\text{If } f_1 = M_2, f_2 = N_2, f_3 = T_2, f_4 = H_2, \\ &\qquad \text{then } \dot{x} = A_{(11)}\mathrm{x} + B_1 w + B_{2(11)}\bar{u}. \\ &\text{If } f_1 = M_1, f_2 = N_2, f_3 = T_1, f_4 = H_2, \\ &\qquad \text{then } \dot{x} = A_{(12)}\mathrm{x} + B_1 w + B_{2(12)}\bar{u}. \\ &\text{If } f_1 = M_2, f_2 = N_1, f_3 = T_1, f_4 = H_2, \\ &\qquad \text{then } \dot{x} = A_{(13)}\mathrm{x} + B_1 w + B_{2(13)}\bar{u}. \\ &\text{If } f_1 = M_2, f_2 = N_1, f_3 = T_2, f_4 = H_1, \\ &\qquad \text{then } \dot{x} = A_{(14)}\mathrm{x} + B_1 w + B_{2(14)}\bar{u}. \\ &\text{If } f_1 = M_2, f_2 = N_1, f_3 = T_2, f_4 = H_2, \\ &\qquad \text{then } \dot{x} = A_{(15)}\mathrm{x} + B_1 w + B_{2(15)}\bar{u}. \\ &\text{If } f_1 = M_2, f_2 = N_2, f_3 = T_1, f_4 = H_2, \\ &\qquad \text{then } \dot{x} = A_{(16)}\mathrm{x} + B_1 w + B_{2(16)}\bar{u}, \end{aligned}$$

where $A_{(i)}$ $(i = 1, 2, 3, \ldots, 16)$. $(i = 1, 2, 3, \ldots, 16)$ are obtained by replacing $f_{(i)}$ $(i = 1, 2)$ in matrix A of (12) with $f_{(i)max}$ and $f_{(i)min}$, respectively. Then the T-S fuzzy model for the nonlinear quarter-car under the bounded state variables is obtained as:

$$\begin{aligned} \dot{x} &= \sum_{i=1}^{16} h_i \left[A_{(i)}\mathrm{x} B_1 w + B_{2(i)}\bar{u} \right] \\ &= A_h \mathrm{x} + B_1 w + B_{2h}\bar{u}, \end{aligned} \tag{16}$$

where

$$\begin{aligned} A_h &= \sum_{i=1}^{16} h_i A_{(i)}, \\ B_{2h} &= \sum_{i=1}^{16} h_i B_{2(i)}, \\ h_1 &= M_1N_1T_1H_1, \quad h_2 = M_1N_1T_1H_2, \\ h_3 &= M_1N_1T_2H_1, \quad h_4 = M_1N_1T_2H_2, \\ h_5 &= M_1N_2T_1H_1, \quad h_6 = M_1N_2T_2H_1, \\ h_7 &= M_1N_2T_2H_2, \quad h_8 = M_2N_1T_1H_1, \\ h_9 &= M_2N_2T_1H_1, \quad h_{10} = M_2N_2T_2H_1, \\ h_{11} &= M_2N_2T_2H_2, \quad h_{12} = M_1N_2T_1H_2, \\ h_{13} &= M_2N_1T_1H_2, \quad h_{14} = M_2N_1T_2H_1, \\ h_{15} &= M_2N_1T_2H_2, \quad h_{16} = M_2N_2T_1H_2, \end{aligned}$$

and $h_{(i)}$ $(i = 1, 2, 3, \ldots, 16)$ satisfy: $\sum_{i=1}^{16} h_{(i)} = 1$.

B. STATE OBSERVER DESIGN

In practice, not all the state variables are available to be measured in real-time. In particular, the evolutionary variable z_d and the absolute displacement, unsprung mass displacement, are nearly unmeasurable while a vehicle is working; direct integration from acceleration to estimate the vertical-velocities deteriorates the accuracy of the estimation consequence. These variables are difficult to be obtained by the

normal instrumentation of a vehicle, which typically only has accelerometers and displacement sensors to be installed. To meet input requirements, a controller must be constructed using the estimated state variables and premise variables; that is, to estimate the state variables in real-time, a state observer is designed and integrated with the controller. In terms of the quarter-car suspension, both the tyre deflection, $z_u - z_r$, and the suspension deflection (SD), $z_s - z_u$, can be measured by laser displacement sensors; the sprung mass acceleration (SMA), $\ddot{z}_s$, and the unsprung mass acceleration, $\ddot{z}_u$, also can be measured by accelerometers. Therefore, the observer measurement is defined as

$$\begin{aligned} Y &= \begin{bmatrix} \ddot{z}_s & \ddot{z}_u & z_s - z_u & z_u - z_r \end{bmatrix}^T \\ &= C_1 \cdot x, \end{aligned} \tag{17}$$

where

$$C_1 = \begin{bmatrix} \frac{c_{01a} + c_{02a}}{-m_s} & \frac{-c_{01a}}{-m_s} & \frac{-c_{02a}}{-m_s} & \frac{k_{01} + k_{s1} + k_{02}}{-m_s} \\ \frac{c_{01a}}{m_u} & \frac{-c_{01a}}{m_u} & 0 & \frac{k_{01}}{m_u} \\ 0 & 0 & 0 & 0 \\ 0 & 0 & 0 & 0 \end{bmatrix}$$
$$\begin{bmatrix} \frac{-k_{s1} - k_{02}}{-m_s} & 0 & \frac{a_{1a}}{-m_s} & \frac{a_{2a}}{-m_s} \\ \frac{k_{s2}}{m_u} & \frac{-k_t}{m_u} & \frac{a_{1a}}{m_u} & 0 \\ 1 & 0 & 0 & 0 \\ 0 & 1 & 0 & 0 \end{bmatrix}.$$

To effectively estimate the state by using the easily measured signals, the estimation error can be defined based on the observer measurement as

$$e = x - \hat{x}. \tag{18}$$

So, the state observer can be designed as

$$\begin{aligned} \dot{\hat{x}} &= \sum_{i=1}^{16} h_i \left[A_{(i)}\hat{x} + L\left(Y - \hat{Y}\right) + B_{2(i)}\overline{u} \right] \\ &= A_h\hat{x} + L\left(Y - \hat{Y}\right) + B_{2h}\overline{u}, \end{aligned} \tag{19}$$

where L are the state observer gains to be designed. Re-arrangement of (19) gives

$$\dot{\hat{x}} = (A_h - LC_1)\,\hat{x} + LY + B_{2h}\overline{u} \tag{20}$$

By differentiating (18), we get the dynamic equation of the state estimation error

$$\begin{aligned} \dot{e} &= \dot{x} - \dot{\hat{x}} \\ &= (A_h - LC_1)\,e + B_1 w. \end{aligned} \tag{21}$$

C. THE DESIGN OF H∞ ROBUST CONTROLLER WITH MULTI-OBJECTIVE OPTIMISATION

The $H\infty$ controller design and stability analysis of fuzzy systems based on T-S state-space model were proposed. By applying the parallel distributed compensation scheme [30] to the MIMO nonlinear system, the observer-based controller can be represented as

$$\begin{aligned} \overline{u} &= \sum_{i=1}^{16} h_i K_{(i)}\hat{x} \\ &= K_h\hat{x}, \end{aligned} \tag{22}$$

where $K_{(i)}$ are the state feedback gains to be designed. Now consider the augmented state vector as

$$\overline{x} = \begin{bmatrix} \hat{x} & e \end{bmatrix}^T. \tag{23}$$

After manipulation, the augmented system can be expressed as the following form:

$$\begin{aligned} \dot{\overline{x}} &= \sum_{i=1}^{16} h_i \left(\overline{G}_{(i)}\overline{x} + \overline{B}_1 w \right) \\ &= \overline{G}_x\overline{x} + \overline{B}_1 w, \end{aligned} \tag{24}$$

where

$$\overline{G}_h = \begin{bmatrix} A_h + B_{2h}K_h & -B_{2h}K_h \\ 0 & A_h - LC_1 \end{bmatrix},$$
$$\overline{B}_1 = \begin{bmatrix} B_1^T & B_1^T \end{bmatrix}^T.$$

For the design of a vehicle suspension, ride comfort, suspension deflection and road holding ability are often regarded as the main optimizing goal in a controller design. To improve the specific performances of the suspension, the controlled output s in this research can be composed of SMA, SD, tyre load (TL) as $\ddot{z}_s$, $z_s - z_u$, and $k_t\,(z_u - z_r)$, respectively, and the values of the weighting parameters σ_1, σ_2, and σ_3 should be set with suitable trade-off and normalization. Therefore, the controlled output is defined as

$$\begin{aligned} s &= \begin{bmatrix} \sigma_1\ddot{z}_s & \sigma_2\,(z_s - z_u) & \sigma_3 k_t\,(z_u - z_r) \end{bmatrix}^T \\ &= \overline{C}_2\overline{x}, \end{aligned} \tag{25}$$

where

$$\overline{C}_2 = \begin{bmatrix} \frac{\sigma - 1(c_{01a} + c_{02a})}{-m_s} & \frac{-\sigma \cdot c_{01a}}{-m_s} & \frac{-\sigma \cdot c_{02a}}{-m_s} & \frac{\sigma_1\,(k_{01} + k_{s1} + k_{02})}{-m_s} \\ 0 & 0 & 0 & \sigma_2 \\ 0 & 0 & 0 & 0 \end{bmatrix}$$
$$\begin{bmatrix} \frac{\sigma_1\,(k_{s1} + k_{02})}{m_s} & 0 & \frac{\sigma_1 \cdot \sigma_{1a}}{-m_s} \frac{\sigma_1 \cdot \sigma_{2a}}{-m_s} & 0_{1\times 8} \\ 0 & 0 & 0 & 0_{1\times 8} \\ 0 & \sigma_3 k_t & 0 & 0_{1\times 8} \end{bmatrix}.$$

In order to give the controller adequate response performance under different vibration situations, the $H\infty$ norm is chosen as the performance measure. The L_2 gain of the system (24) with (25) is defined as

$$\|T_{sw}\|_\infty = \sup_{\|w\|_2 \neq 0} \frac{\|s\|_2}{\|w\|_2}, \tag{26}$$

where $\|s\|_2^2 = \int_0^\infty s^T(t)\,s(t) \cdot dt$ and $\|w\|_2^2 = \int_0^\infty w^T(t)\,w(t) \cdot dt$.

The aim of the work is to design a fuzzy controller, equation (22), such that the closed-loop fuzzy system, equation (24), is quadratically stable. A Lyapunov function for the system (24) is defined as

$$\Pi(\overline{x}) = \dot{x}^T P \overline{x}, \tag{27}$$

where P is a positive definite matrix and $P = P^T$. By differentiating (27), we obtain

$$\dot{\Pi}(\overline{x}) = \dot{x}^T P \overline{x} + \overline{x}^T P \dot{\overline{x}}. \tag{28}$$

Adding $s^T \mathrm{s} - \gamma^2 w^T w$ to the two sides of (28) yields

$$\begin{aligned}\dot{\Pi}(\overline{x}) + s^T \mathrm{s} - \gamma^2 w^T w \\ = \overline{x}^T P \overline{x} + \overline{x}^T P \dot{\overline{x}} + s^T s - \gamma^2 w^T w.\end{aligned} \tag{29}$$

Substituting (24) and (25) into (29) gives

$$\begin{aligned}&\dot{\Pi}(\overline{x}) + s^T \mathrm{s} - \gamma^2 w^T w \\ &= \left(\overline{G}_h \overline{x} + \overline{B}_1 w\right)^1 P \overline{x} + \overline{x}^T P \left(\overline{G}_h \overline{x} + \overline{B}_1 w\right) \\ &\quad + \left(\overline{C}_2 \overline{x}\right)^T \left(\overline{C}_2 \overline{x}\right) - \gamma^2 w^T w.\end{aligned} \tag{30}$$

Re-arrangement of (30) gives

$$\begin{aligned}&\dot{\Pi}(\overline{x}) + s^T \mathrm{s} - \gamma^2 w^T w \\ &= \begin{bmatrix} \overline{x}^T \\ w^T \end{bmatrix} \begin{bmatrix} \overline{G}_h^T P + P \overline{G}_h + \overline{C}_2^T \overline{C}_2 & P\overline{B}_1 \\ * & -\gamma^2 \end{bmatrix} \begin{bmatrix} \overline{x} \\ w \end{bmatrix}.\end{aligned} \tag{31}$$

Considering

$$\Psi = \begin{bmatrix} \overline{G}_h^T P + P \overline{G}_h + \overline{C}_2^T \overline{C}_2 & P\overline{B}_1 \\ * & -\gamma^2 \end{bmatrix}, \tag{32}$$

when the disturbance is zero, that is, $w = 0$, it can be inferred from (31) and (32) that if $\Psi < 0$, then $\dot{\Pi}(\overline{x}) < 0$, and the closed-loop fuzzy system (24) is quadratically stable. By considering Schur complement equivalence, equation (32) can be further re-arranged to linear matrix inequalities (LMIs), as given below:

$$\Psi = \begin{bmatrix} \overline{G}_h^T P + P \overline{G}_h & \overline{C}_2^T & P\overline{B}_1 \\ * & -I & 0 \\ * & * & -\gamma^2 \end{bmatrix} < 0, \tag{33}$$

where I is a unit matrix.

Considering the input saturation in (22) with the assumption that $u_{\lim} = u_{\max} = -u_{\min}$, the input constraint can be expressed based on the lemma in [30] as

$$\left| \sum_{i=1}^{16} K_i \hat{x} \right| \leqslant \frac{u_{\lim}}{\varepsilon}, \tag{34}$$

where $0 < \varepsilon < 1$ is a given scalar. If $\left|K_i \hat{x}\right| \leqslant \left(u_{\lim} / \varepsilon\right)$, then (34) holds. Let

$$\Omega(K) = \left\{ \hat{x} \middle| |\hat{x}^{\mathrm{T}} K_i^{\mathrm{T}} K_i \hat{x}| \leqslant \left(\frac{u_{\lim}}{\varepsilon}\right)^2 \right\},$$

the equivalent condition for $\Omega(P, \rho) = \left\{\hat{x} | \hat{x}^{\mathrm{T}} P \hat{x} \leqslant \rho\right\}$ being a subset of $\Omega(K)$ is:

$$K_i \left(\frac{P}{\rho}\right)^{-1} K_i^{\mathrm{T}} \leqslant \left(\frac{u_{\lim}}{\varepsilon}\right)^2. \tag{35}$$

By applying Schur complement equivalence, (35) can be written as

$$\begin{bmatrix} \left(\frac{u_{\lim}}{\varepsilon}\right)^2 & K_i \left(\frac{P}{\rho}\right)^{-1} \\ \left(\frac{P}{\rho}\right)^{-1} K_i^{\mathrm{T}} & \left(\frac{P}{\rho}\right)^{-1} \end{bmatrix} \geq 0. \tag{36}$$

It should be noted that the input current sent to the MR damper is generally $0 \sim I_{\max}$, which means $I_{\min} = 0$, and an asymmetric saturation should be considered. Therefore, the assumption of symmetric saturation in (36) should be modified to shift the saturation centre as the average of both saturation limits. In this paper, the input currents are considered to be $I_1 : 0\mathrm{A} \sim 0.4\mathrm{A}$ and $I_2 : 0\mathrm{A} \sim 1\mathrm{A}$; hence, to design the controller, we define $u_{\lim} = (u_{\min} + u_{\max})/2$ with $u_{\min} = 0$, that is $I_{1\,\lim} = 0.2\mathrm{A}$ and $I_{2\,\lim} = 0.5\mathrm{A}$.

To ensure the T-S fuzzy system (12) with the controller (22) is quadratically stable and for a given parameter $\gamma > 0$, the L_2 gain defined by (26) is less than γ, the matrices $Q > 0$, $Y > 0$, where $Q = P^{-1}$ and $Y = KQ$, should exist such that (33) and (36) are satisfied. Hence, to minimize the performance measure parameter γ, the controller design issue can be modified as a minimization problem of

$$\begin{aligned}&\min \gamma^2 \\ &\textit{subject to}\ \text{LMIs (33) } \textit{and}\ \text{(36)}.\end{aligned} \tag{37}$$

By solving the LMIs using MATLAB® software, the state feedback $\mathrm{K}_{(i)}$ gains and the observer gains $L_{(i)}$ of TSFH controller are determined. By fusion of the T-S Fuzzy model and $H\infty$ techniques, the algorithm proposed in this paper can provide a direct control for nonlinear MIMO system without the problem ''coupled interconnections'', which leads to a much simpler controller with less computational load, and it is easy to be implemented in real applications.

After constructing the controller, the T-S fuzzy model is left aside in the simulation work, and the closed-loop control system is shown in Fig. 3. For the convenience of the reader, the modules of TSFH controller, the quarter-car system, and processing signals are represented by blue blocks, grey block, and lines with the arrow, respectively. It can be seen that the measured parameters, $\ddot{z}_s$, $\ddot{z}_u$, $z_s - z_u$ and $z_u - z_r$, are transmitted to the state observer, and thus the estimated complete state variables can be determined. By running the control algorithm based on the inputs consisted of the eight estimated variables, the controller calculates command currents with the consideration of actuator saturation and sends them to the two MR dampers which belong variable damping module and variable stiffness module, respectively.

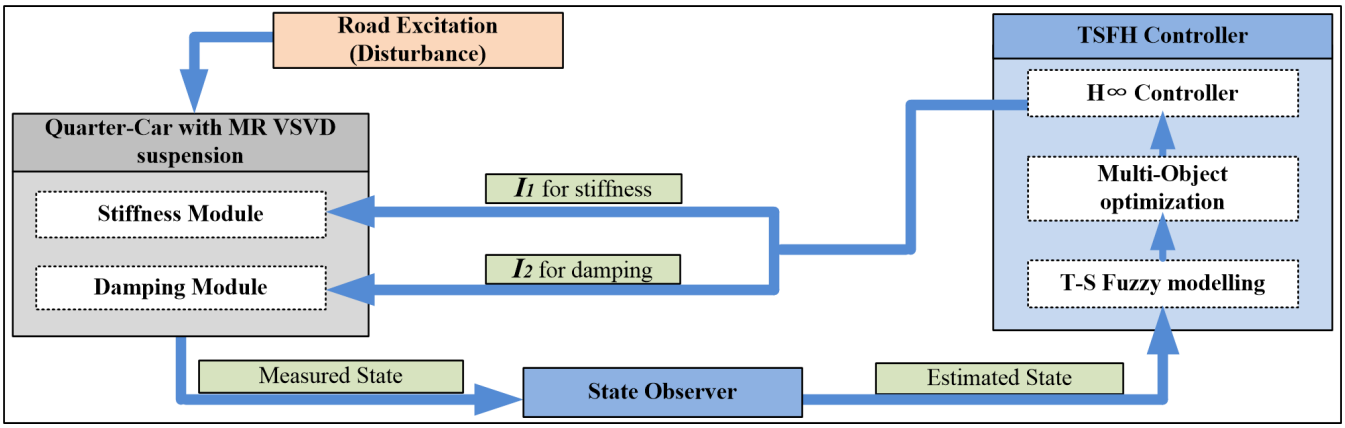

FIGURE 3. The control flow of the VSVD quarter-car system.

IV. NUMERICAL APPLICATION

In this section, the proposed method is applied to design a controller for the quarter-car model with the MR VSVD suspension as described in section II and the values of the suspension model parameters are listed in Table 1. In section IV-A, two kinds of road profiles will be established as the disturbance to the tire, and a competing controller will also be described in this part. Then, the designed TSFH controller will be applied for the quarter-car with MR VSVD suspension and validated in section IV-B. In the simulation, it is assumed that only the $\ddot{z}_s$, $\ddot{z}_u$, $z_s - z_u$, and $z_u - z_r$ are available for measurement and all the state variables defined in (4) will be estimated.

A. ROAD EXCITATION AND COMPETING CONTROLLER

In the simulation work, two typical road profiles are considered. A bump input, which is normally used to describe the transient response characteristic, is adopted as the first road excitation. The corresponding road displacement is given by

$$z_r(t) = \begin{cases} \frac{a}{2}\left[1 - \cos\left(\frac{2\pi v_0}{l}t\right)\right], & 0 \le t \le \frac{l}{v_0}, \\ 0, & t > \frac{l}{v_0}, \end{cases} \tag{38}$$

where $a = 0.07$m and $l = 0.8$m are chosen as the height and length of the bump, and the vehicle forward velocity as $v_0 = 0.856 m/s$ [30]. The bump road profile in the time domain is demonstrated in Fig. 4(a).

The second type of road excitation, normally used to evaluate frequency response, is a random road excitation. The standard C class road profile (ISO 8608), with $S_q(\Omega_o) = 16 \times 10^{-6} m^3$, is generated with the sinusoidal approximation method [31]. The road irregularities can be described by the following equation

$$z_r(t) = \sum_{i=1}^{n} \left(\sqrt{2S_q(i\Delta\Omega)\,\Delta\Omega}\right) \sin(i2\pi\,\Delta\Omega v_r t + \varphi_i), \tag{39}$$

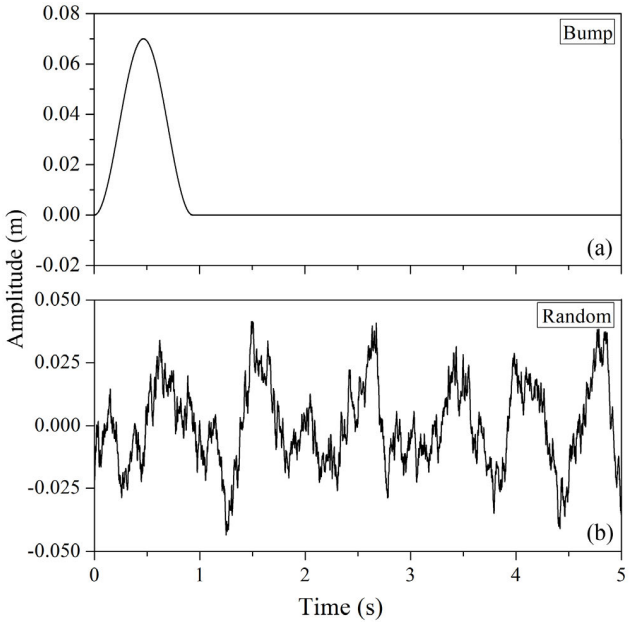

FIGURE 4. Test excitation (a) the bump road profile and (b) the random road profile.

where φ_i is the random numbers distributed uniformly among $[0, 2\pi]$, $\Delta\Omega$ is the minimum spatial frequency value we considered, which equals to $0.011 m^{-1}$. In this work, the vehicle is assumed to travel with a constant speed $v_r = 20$m/s over a given road segment, and conducted under the class C road profile, which is shown in Fig. 4(b) in the time domain.

To validate the performance of the TSFH, a damping and stiffness independent controller (IC) is adopted for a comparison. As the stiffness and the damping of the suspension are adjusted and controlled independently, for the variable damping module, a classic skyhook controller (sub controller 1 of IC) is applied, which is simple while effective. The description for skyhook controller is

$$F_{sky} = \begin{cases} C_{max}\dot{z}_s, & \dot{z}_s(\dot{z}_s - \dot{z}_u) \ge 0, \\ C_{min}\dot{z}_s, & \dot{z}_s(\dot{z}_s - \dot{z}_u) < 0, \end{cases} \tag{40}$$

where C_{max} and C_{min} are the maximum and minimum sky-hook gains, which correspond to the command currents I_{max} and I_{min}, respectively. In this experiment, the specific sky-hook force is expressed as the MR damper force with the control output current, I_{max}=1A and $I_{min} = 0$A. In terms of the control strategy for the stiffness component, it is to avoid the resonance of the quarter car under a pavement input. As the stiffness is controlled according to the dominant excitation frequency, the controller for variable stiffness module (sub controller 2 of IC) is presented as follows

$$k_s = \begin{cases} k_{max}\ (I_s = 0.4A)\,, & f_{req} < f_c OR\, |z_s - z_u| \geq s_t, \\ k_{min}\ (I_s = 0\text{A})\,, & \text{Otherwise}, \end{cases} \tag{41}$$

where f_c is the switching frequency determined as 1.51 Hz, f_{req} is the dominant frequency of the pavement input signal collecting from a state observer in real time. More design details about this controller can be found in [28].

To validate the effectiveness of the designed controller in the simulation, the MR VSVD suspension model will be used to represent the real suspension in a quarter-car system. The parameter values of the linear quarter-car model described in (2) are listed in Table 2.

TABLE 2. Parameter values of the quarter-car model [28].

Symbol	Value	Unit
k_s	16905	N / m
k_t	179000	N / m
m_s	257.6	kg
m_u	33.2	kg
c_s	800	N · s / m

B. NUMERICAL RESULTS

By applying the two kinds of road profiles to the quarter-car with MR VSVD suspension, the system response without control (Passive), the response with IC controlled, and the response with TSFH controlled are evaluated.

In the first stage of the simulation, bump road is carried out to evaluate the systems. The bump responses, input currents for two MR modules, and corresponding MR damper forces are shown in Figs. 5-7, respectively. Time histories of the test rig response in terms of the three performance criteria, SMA, SD, TL, are recorded and plotted in Fig. 5. It can be seen from Fig. 5 that better responses are obtained for the controlled MR VSVD suspensions compared to the passive one. In order to illustrate the simulation results more clearly, the responses of the three suspensions are compared in Table 3 in terms of the peak-to-peak (PTP) values and the improved percentages compared to the passive suspension. It can be seen from the first row of Table 3 that the two controlled MR VSVD suspensions perform much better than passive suspension on SMA, and the response of TSFH comparing to Passive, 37.1%, is outstanding smaller than that of IC control, 20.3%. Regarding the time response shown in the third row of Table 3, the PTP value of tyre load fluctuation of TSFH is smaller than that of passive by approximately 34.1%, which is much more effective comparing to 10.8% of IC control.

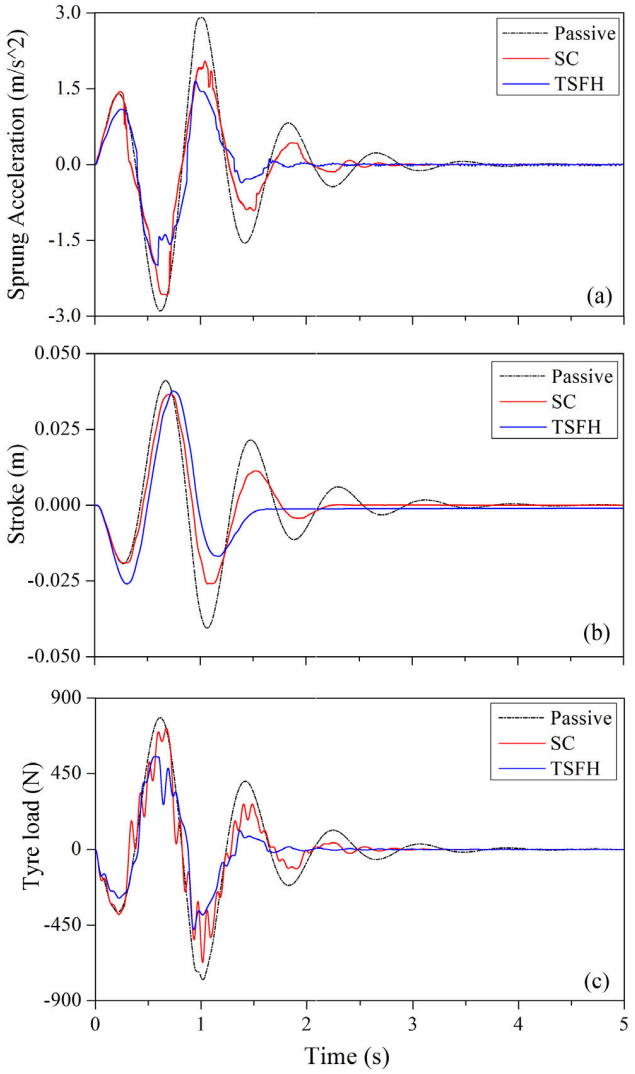

FIGURE 5. Response under the bump road (a) response of SMA, (b) response of SD, and (c) response of TL.

TABLE 3. PTP value of objectives under bump road profile.

Objective	Passive	IC	TSFH
SMA PTP (m/s^2)	5.81	4.63	3.65
Reduction (%)	N/A	-20.3	-37.1
SD PTP (m)	0.0817	0.0624	0.0636
Reduction (%)	N/A	-23.6	-22.2
TL PTP (N)	1555	1387	1026
Reduction (%)	N/A	-10.8	-34.1

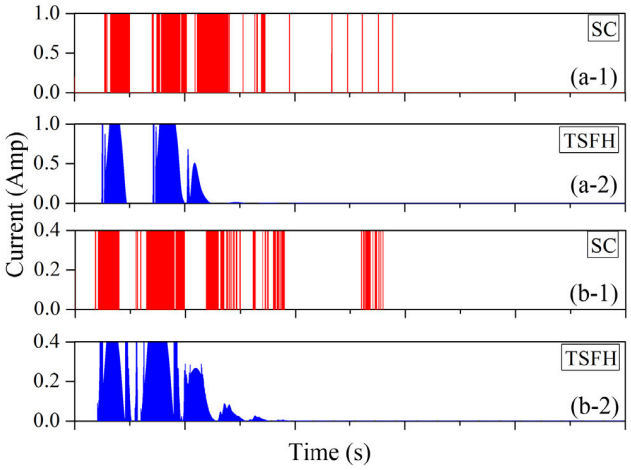

FIGURE 6. Input current under the bump road (a-1) IC/damping, (a-2) TSFH/damping, (b-1) IC/stiffness, and (b-2) TSFH/stiffness.

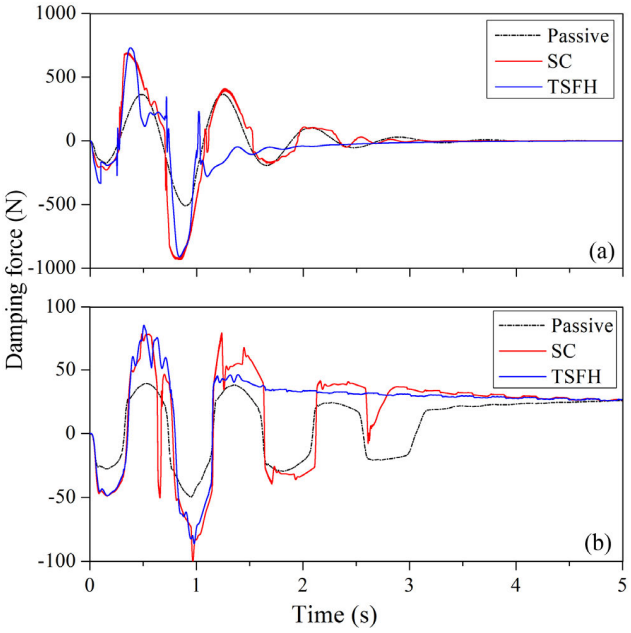

FIGURE 7. MR Damper force under the bump road (a) damping module and (b) stiffness module.

Figs. 6 and 7 show the input currents of IC and TSFH and the corresponding damping forces generated by the MR dampers under the bump road profile excitation, respectively. In Fig. 6, the two controllers' input currents for damping module and stiffness module are separately shown in subfigures for clarity. It is also presented from Fig. 6 that the current signals obtained from TSFH is continuously varied and is almost zero when the system responses reach the steady state. On the contrary, the current signals computed from IC control are discrete values. Furthermore, due to the sensitivity of Heaviside step function to small errors between the desired force and the measured force, the control current of IC is not always zero even when the system responses reach the steady state.

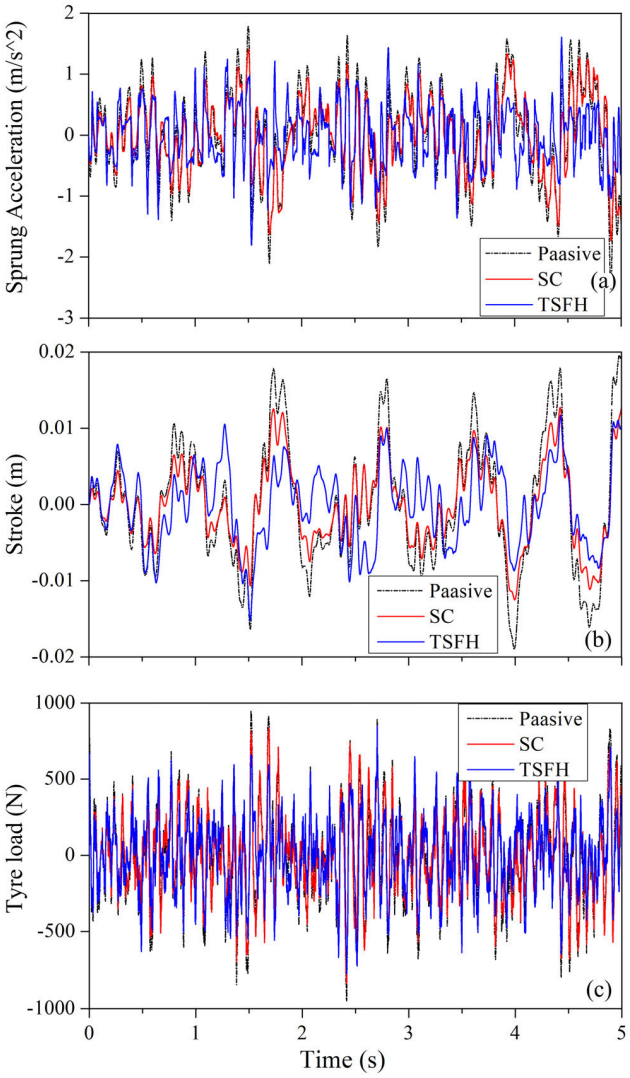

FIGURE 8. Response under the random road (a) response of SMA, (b) response of SD, and (c) response of TL.

After the bump road evaluation, random road evaluation is further conducted. Time histories of the quarter-car system under random road excitation are recorded and plotted in Fig. 8, where the results of SMA, SD, TL, are shown in the subfigures, respectively. In particular, the SMA under the passive case has the biggest peak value during the whole-time history. TSFH case and IC case both perform better than the passive case. However, the SMA with TSFH case is further reduced than with IC case.

It means that the quarter-car system performs best under the TSFH suspension where the damping and the stiffness of the damper are both controlled in real time. It is noted from the figure that the MR VSVD suspension controlled by TSFH further limits and inhibits the variation of the specific objectives compared to the passive one and the system controlled by IC. Whereas under excitation with wide-band frequency such as random road profile, the filtering performance of independent control method is worse, or even like

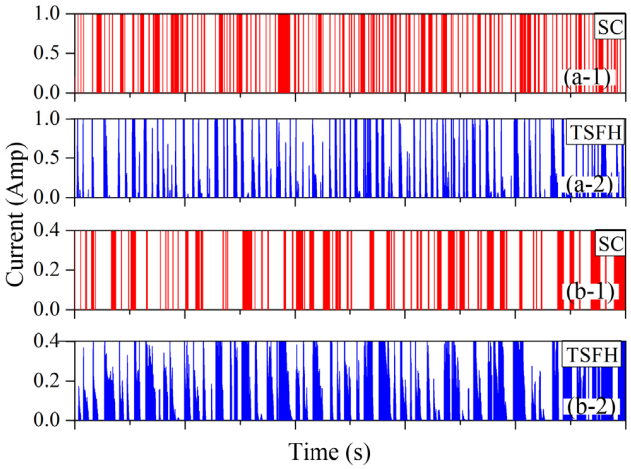

FIGURE 9. Input current under the random road (a-1) IC/damping, (a-2) TSFH/damping, (b-1) IC/stiffness, and (b-2) TSFH/stiffness.

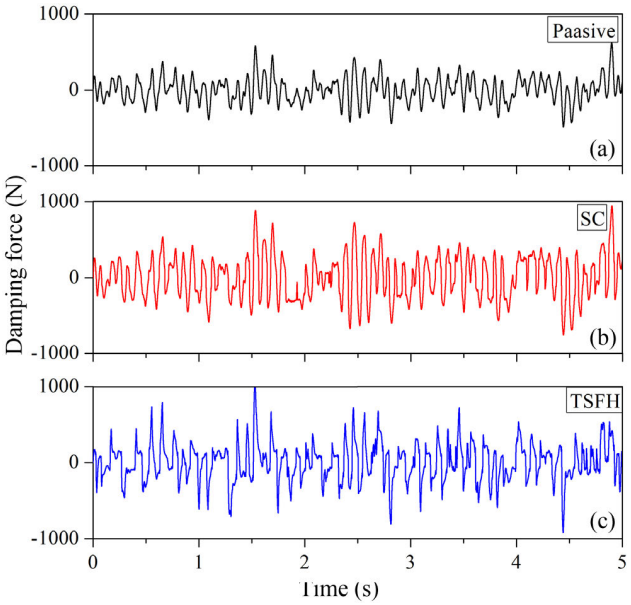

FIGURE 10. The MR Damper force of damping module under the random road.

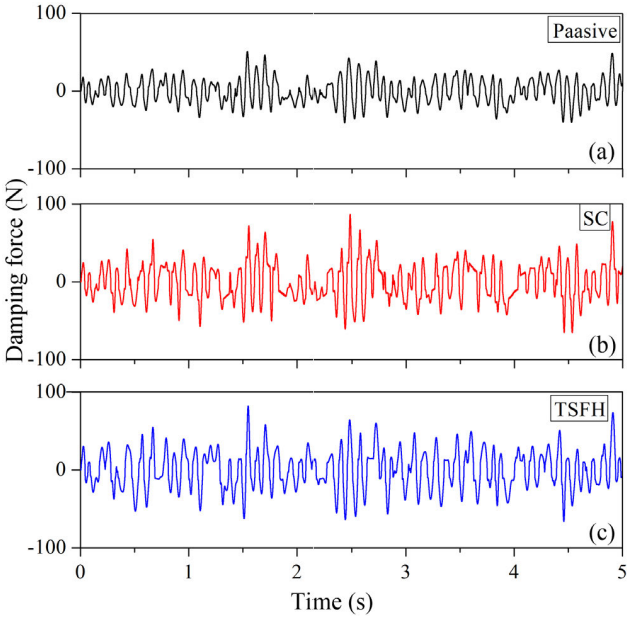

FIGURE 11. The MR Damper force of stiffness module under the random road.

TABLE 4. RMS value of objectives under the random road profile.

Objective	Passive	IC	TSFH
SMA RMS (m/s^2)	0.785	0.619	3.65
Reduction (%)	N/A	-21.2	-37.1
SD RMS (m)	0.00695	0.00466	0.0636
Reduction (%)	N/A	-32.9	-22.2
TL RMS (N)	318.87	289.04	1026
Reduction (%)	N/A	-9.4	-34.1

the performance of a passive suspension. It might be due to the coupled interconnections phenomenon of multi-output which has been noted in section I. On the contrary, to control the MR VSVD suspension, a MIMO system with high nonlinearity, the TSFH controller based on T-S fuzzy model and $H\infty$ control has presented further better performance under a complex excitation with multi-frequency components.

To further demonstrate the performance of TSFH, the root-mean-square (RMS) values of the system responses are summarized in Table 4 and the controlled MR suspension with the TSFH has the lowest RMS value of the SMA. In particular, the suspension controlled by TSFH can reduce the RMS values for SMA, SD, and TL by about 27.6%, 22.0%, and 15.8%, respectively, compared with the passive suspension. The SMA and TL reductions (-27.6% and -15.8%) of TSFH are more effective than the ones of the typical IC control (-21.2% and -9.4%). These results demonstrate that under complex wide-frequency external disturbance, TSFH control can further overcome the nonlinearity and multi-output coupling problems of the MR VSVD suspension system, comparing to the separated control method. Regarding the SD RMS values, the TSFH control is $5.42 \times 10^{-3}m$, of which one fails than the IC control, $4.66 \times 10^{-3}m$. The indistinctive SD effect of TSFH might be attributed to its multi-output control method, which aims at the global optimum with the consideration of coupled interconnections between the damping module and stiffness module.

Fig. 9 demonstrates the input currents of IC and TSFH for damping module and stiffness module, respectively. The damping forces generated by the two modules under the random road profile excitation are shown in Figs. 10 and 11. In the two figures, the damping forces of Passive, IC, and TSFH are separately shown in subfigures for clarity.

V. CONCLUSION

A T-S Fuzzy model-based H∞ controller for multi-MR VSVD suspension was successfully designed in this study. The MR suspension system is a MIMO nonlinear system containing input hysteresis nonlinearity, time-varying delays, model uncertainties, and external disturbances. The proposed T-S Fuzzy model can predict the stiffness and damping variation characteristics of the VSVD MR suspension. Based on the T-S fuzzy model, an H∞ controller under an optimisation on multiple objectives can be designed to improve suspension performance. A fuzzy state observer design is proposed to estimate the suspension state in real-time so that the implementation of the control system is feasible in practical application. Numerical simulations were conducted under bump and random excitation. The results show that the VSVD MR suspension system with TSFH controller performs better in improving the multiple driving indicators including riding comfort and vehicle stability to the passive system and IC control system. The results illustrate the TSFH with damping and stiffness synchronic multi-output control on MR VSVD suspension further improves the comfort and robustness of the vehicle system comparing with the damping and stiffness independent controller, with respect to different road input conditions.

APPENDIX

$$A = \begin{bmatrix} \frac{c_{01a}+c_{02a}}{-m_s} & \frac{-c_{01a}}{-m_s} & \frac{-c_{02a}}{-m_s} & \frac{k_{01}+k_{s1}+k_{02}}{-m_s} & \frac{-k_{s1}-k_{02}}{-m_s} & 0 & \frac{a_{1a}}{-m_s} & \frac{a_{2a}}{-m_s} \\ \frac{c_{01a}}{m_u} & \frac{-c_{01a}}{m_u} & 0 & \frac{k_{01}}{m_u} & \frac{k_{s2}}{m_u} & \frac{-k_t}{m_u} & \frac{a_{1a}}{m_u} & 0 \\ \frac{c_{01a}}{m_k} & 0 & \frac{-c_{01a}}{m_k} & \frac{k_{s1}+k_{02}}{m_k} & \frac{-k_{01}-k_{s1}-k_{02}}{m_k} & 0 & 0 & \frac{a_{2a}}{m_k} \\ 1 & -1 & 0 & 0 & 0 & 0 & 0 & 0 \\ 0 & -1 & 1 & 0 & 0 & 0 & 0 & 0 \\ 0 & 1 & 0 & 0 & 0 & 0 & 0 & 0 \\ A_{d1} & -A_{d1} & 0 & 0 & 0 & 0 & 0 & 0 \\ A_{d1} & 0 & A_{d1} & 0 & 0 & 0 & f_1 & 0 \\ & & & & 0 & 0 & 0 & f_2 \end{bmatrix},$$

$$B_1 = \begin{bmatrix} 0 & 0 & 0 & 0 & 0 & -1 & 0 & 0 \end{bmatrix}^T,$$

$$B_2 = \begin{bmatrix} \frac{f_3}{-m_s} & \frac{f_3}{m_u} & \frac{0}{m_k} & 0 & 0 & 0 & 0 & 0 \\ \frac{f_4}{-m_s} & \frac{0}{m_u} & \frac{f_4}{m_k} & 0 & 0 & 0 & 0 & 0 \end{bmatrix}^T.$$

REFERENCES

[1] X. Shao, F. Naghdy, H. Du, and Y. Qin, "Coupling effect between road excitation and an in-wheel switched reluctance motor on vehicle ride comfort and active suspension control," *J. Sound Vib.*, vol. 443, pp. 683–702, Mar. 2019.
[2] D. Ning, H. Du, N. Zhang, S. Sun, and W. Li, "Controllable electrically interconnected suspension system for improving vehicle vibration performance," *IEEE/ASME Trans. Mechatronics*, early access, Jan. 10, 2020, doi: 10.1109/TMECH.2020.2965573.
[3] M. Zapateiro, F. Pozo, H. R. Karimi, and N. Luo, "Semiactive control methodologies for suspension control with magnetorheological dampers," *IEEE/ASME Trans. Mechatronics*, vol. 17, no. 2, pp. 370–380, Apr. 2012.
[4] D. X. Phu, D. K. Shin, and S.-B. Choi, "Design of a new adaptive fuzzy controller and its application to vibration control of a vehicle seat installed with an MR damper," *Smart Mater. Struct.*, vol. 24, no. 8, Aug. 2015, Art. no. 085012.
[5] M. Yu, C. R. Liao, W. M. Chen, and S. L. Huang, "Study on MR semiactive suspension system and its road testing," *J. Intell. Mater. Syst. Struct.*, vol. 17, nos. 8–9, pp. 801–806, Sep. 2006.
[6] S. Sun, X. Tang, J. Yang, D. Ning, H. Du, S. Zhang, and W. Li, "A new generation of magnetorheological vehicle suspension system with tunable stiffness and damping characteristics," *IEEE Trans. Ind. Informat.*, vol. 15, no. 8, pp. 4696–4708, Aug. 2019.
[7] L. M. Jugulkar, S. Singh, and S. M. Sawant, "Analysis of suspension with variable stiffness and variable damping force for automotive applications," *Adv. Mech. Eng.*, vol. 8, no. 5, May 2016, Art. no. 1687814016648638, doi: 10.1177/1687814016648638.
[8] X. Dong, W. Liu, X. Wang, J. Yu, and P. Chen, "Research on variable stiffness and damping magnetorheological actuator for robot joint," in *Proc. ICIRA*, Wuhan, China, 2017, pp. 109–119.
[9] Y. Xu, M. Ahmadian, and R. Sun, "Improving vehicle lateral stability based on variable stiffness and damping suspension system via MR damper," *IEEE Trans. Veh. Technol.*, vol. 63, no. 3, pp. 1071–1078, Mar. 2014.
[10] Y. Xu and M. Ahmadian, "Improving the capacity of tire normal force via variable stiffness and damping suspension system," *J. Terramech.*, vol. 50, no. 2, pp. 121–132, Apr. 2013.
[11] O. M. Anubi and C. D. Crane, "A new active variable stiffness suspension system using a nonlinear energy sink-based controller," *Vehicle Syst. Dyn.*, vol. 51, no. 10, pp. 1588–1602, Oct. 2013.
[12] O. M. Anubi and C. Crane, "A new semiactive variable stiffness suspension system using combined skyhook and nonlinear energy sink-based controllers," *IEEE Trans. Control Syst. Technol.*, vol. 23, no. 3, pp. 937–947, May 2015.
[13] C. Spelta, F. Previdi, S. M. Savaresi, P. Bolzern, M. Cutini, C. Bisaglia, and S. A. Bertinotti, "Performance analysis of semi-active suspensions with control of variable damping and stiffness," *Vehicle Syst. Dyn.*, vol. 49, nos. 1–2, pp. 237–256, Feb. 2011.
[14] T. Yang, N. Sun, H. Chen, and Y. Fang, "Neural network-based adaptive antiswing control of an underactuated ship-mounted crane with roll motions and input dead zones," *IEEE Trans. Neural Netw. Learn. Syst.*, vol. 31, no. 3, pp. 901–914, Mar. 2020.
[15] N. Sun, J. Zhang, X. Xin, T. Yang, and Y. Fang, "Nonlinear output feedback control of flexible rope crane systems with state constraints," *IEEE Access*, vol. 7, pp. 136193–136202, 2019.
[16] N. Sun, Y. Wu, X. Liang, and Y. Fang, "Nonlinear stable transportation control for double-pendulum shipboard cranes with Ship-Motion-Induced disturbances," *IEEE Trans. Ind. Electron.*, vol. 66, no. 12, pp. 9467–9479, Dec. 2019.
[17] Y. Liu, H. Jin, and T. Masaaki, "Ride comfort and wheel load fluctuation compatible control using variable stiffness and damping," in *Proc. FISITA World Automot. Congr.*, Beijing, China, 2012, pp. 355–365.
[18] J. Tang and S. Chen, "Study on periodic solutions of strong nonlinear systems with time-varying damping and stiffness coefficient," *J. Vib. Shock*, vol. 10, no. 1, pp. 96–100, 2007.
[19] X. Shao, F. Naghdy, H. Du, and H. Li, "Output feedback H_∞ control for active suspension of in-wheel motor driven electric vehicle with control faults and input delay," *ISA Trans.*, vol. 92, pp. 94–108, Sep. 2019.
[20] J. Wang, Y. Zhou, and J. Liu, "Hinf loop shaping control for a class of MIMO nonlinear systems," *J. Zhongyuan Univ. Technol.*, vol. 4, p. 2, Jan. 2007.
[21] Y. Yang, D. Constantinescu, and Y. Shi, "Robust four-channel teleoperation through hybrid damping-stiffness adjustment," *IEEE Trans. Control Syst. Technol.*, vol. 28, no. 3, pp. 920–935, May 2020.

[22] A. Fakharian and V. Azimi, "Robust mixed-sensitivity H_∞ control for a class of MIMO uncertain nonlinear IPM synchronous motor via T-S fuzzy model," in *Proc. 17th MMAR*, Miedzyzdroje, Poland, 2012, pp. 546–551.
[23] S. H. Mousavi, B. Ranjbar-Sahraei, and N. Noroozi, "Output feedback controller for hysteretic time-delayed MIMO nonlinear systems," *Nonlinear Dyn.*, vol. 68, nos. 1–2, pp. 63–76, Apr. 2012.
[24] H. Du and N. Zhang, "Model-based fuzzy control for buildings installed with magneto-rheological dampers," *J. Intell. Mater. Syst. Struct.*, vol. 20, no. 9, pp. 1091–1105, Jun. 2009.
[25] K. Tanaka and H. Wang, "Takagi–Sugeno fuzzy model and parallel distributed compensation," in *Fuzzy Control Systems Design and Analysis: A Linear Matrix Inequality Approach*. Hoboken, NJ, USA: Wiley, 2002, pp. 5–48.
[26] G. Rödönyi, "Heterogeneous string stability of unidirectionally interconnected MIMO LTI systems," *Automatica*, vol. 103, pp. 354–362, May 2019.
[27] X. Tang, H. Du, S. Sun, D. Ning, Z. Xing, and W. Li, "Takagi–Sugeno fuzzy control for semi-active vehicle suspension with a magnetorheological damper and experimental validation," *IEEE/ASME Trans. Mechatronics*, vol. 22, no. 1, pp. 291–300, Feb. 2017.
[28] X. Tang, "Advanced suspension system using magnetorheological technology for vehicle vibration control," Ph.D. dissertation, Dept. Mech. Eng., Univ. Wollongong, Wollongong, NSW, Australia, 2018.
[29] D. H. Wang and W. H. Liao, "Magnetorheological fluid dampers: A review of parametric modelling," *Smart Mater. Struct.*, vol. 20, no. 2, Feb. 2011, Art. no. 023001.
[30] H. Du, J. Lam, K. C. Cheung, W. Li, and N. Zhang, "Direct voltage control of magnetorheological damper for vehicle suspensions," *Smart Mater. Struct.*, vol. 22, no. 10, Oct. 2013, Art. no. 105016.
[31] F. Tyan, Y. Hong, S. Tu, and W. Jeng, "Generation of random road profiles," *J. Adv. Eng.*, vol. 4, no. 2, pp. 1373–1378, 2009.

XIN TANG (Member, IEEE) received the B.E. degree in automation engineering from the University of Electronic Science and Technology of China, Chengdu, China, in 2012, and the Ph.D. degree from the School of Mechanical, Material and Mechatronics, University of Wollongong, Wollongong, NSW, Australia, in 2018.

He is currently a Research Fellow with the HKUST Fok Ying Tung Research Institute. His research interests include the vibration control of semiactive vehicle suspension utilizing MR technology, robust control applications, and human-like algorithms to enhance decision-making modeling for local path planning and trajectory tracking control.

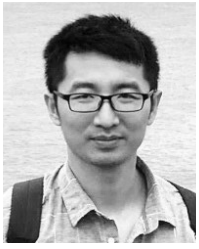

DONGHONG NING (Member, IEEE) received the B.E. degree in agricultural mechanization and automation from the College of Mechanical and Electronic Engineering, North West Agriculture and Forestry University, Yangling, China, in 2012, and the Ph.D. degree from the University of Wollongong, Australia, in 2018.

His research interests include active and semi-active vibration control, multiple degrees of freedom vibration control, interconnected suspension, electromagnetic suspension, and mechanical–electrical networks.

HAIPING DU (Senior Member, IEEE) received the Ph.D. degree in mechanical design and theory from Shanghai Jiao Tong University, Shanghai, China, in 2002.

He was a Research Fellow with the University of Technology, Sydney, from 2005 to 2009, and was a Postdoctoral Research Associate with Imperial College London, from 2004 to 2005 and the University of Hong Kong, from 2002 to 2003. He is currently a Professor with the School of Electrical, Computer and Telecommunications Engineering, University of Wollongong, Wollongong, NSW, Australia.

Dr. Du was a recipient of the Australian Endeavour Research Fellowship, in 2012. He is a Subject Editor of the *Journal of Franklin Institute*, an Associate Editor of IEEE Control Systems Society Conference, an Editorial Board Member for some international journals, such as the *Journal of Sound and Vibration*, the *IMechE Journal of Systems and Control Engineering*, the *Journal of Low Frequency Noise, Vibration, and Active Control*, and a Guest Editor of *IET Control Theory and Application*, *Mechatronics*, and *Advances in Mechanical Engineering*.

WEIHUA LI (Member, IEEE) received the B.E. and M.E. degrees from the University of Science and Technology of China, Hefei, China, in 1992 and 1995, respectively, and the Ph.D. degree from Nanyang Technological University, Nanyang, Singapore, in 2001.

He was with the School of Mechanical and Production Engineering, Nanyang Technological University, as a Research Fellow, from 2001 to 2003. He has been with the School of Mechanical, Materials and Mechatronic Engineering, University of Wollongong, Wollongong, NSW, Australia, as an Academic Staff Member, since 2003. He has published more than 350 technical articles in refereed international journals and conferences.

Prof. Li received the number of awards, including the JSPS Invitation Fellowship in 2014, the Endeavour Research Fellowship in 2011, and the Scientific Visits to China Program Awards. He serves as an Associate Editor or Editorial Board Member for nine international journals.

YIBO GAO received the B.E. degree from Zhejiang Forest University, Hangzhou, China, in 2010, the M.E. degree from Zhejiang University, Hangzhou, in 2013, and the Ph.D. degree from the Hong Kong University of Science and Technology, in 2017.

He is interested in the development of novel Bio-MEMS chip technology, including silicon-based chip design, fabrication, packaging and testing for various biological and clinical applications. Especially, his research areas focus on microfluidics chip design and fabrication technology and its application in fundamental biological research and diagnostic technology, such as PCR molecular detection, single molecule detection, and liquid biopsy in cancer early detection.

WEIJIA WEN received the B.E. and M.E. degrees from Chongqing University, Chongqing, China, in 1992 and 1995, respectively, and the Ph.D. degree from the Institute of Physics, Chinese Academy of Sciences, China, in 1995.

From 1995 to 1999, he was a Research Fellow with the Hong Kong University of Science and Technology (HKUST) and UCLA. Since 1999, he has been with the Department of Physics, Hong Kong University of Science and Technology, Hong Kong as an Academic Staff Member. He has published more than 400 articles in his major research fields, including more than 350 journal article and 50 conference invited report. So far, more than 300 SCI articles have been published. His refereed journal articles have been cited more than 10 500 times resulting in an H-index of 52. His main research interests include soft condensed matter physics, electrorheological (ER) and magnetorheological (MR) fluids, field-induced pattern and structure transitions, micro- and nano-fluidic controlling, advanced functional materials including microsphere and nanoparticle fabrications, thin film physics, band gap materials, metamaterials, and nonlinear optical materials.